Pulse repetition rate effect on the intensity inside femtosecond laser filament in air

Fukang Yin[1,2], Juan Long[1,2], Yaoxiang Liu[1,*], Yingxia Wei[1], Bin Zhu[3] , Kainan Zhou[3], Tie-Jun Wang[1,2,*], Yuxin Leng[1,2], AND Ruxin Li[1,2]

[1] *State Key Laboratory of High Field Laser Physics, Shanghai Institute of Optics and Fine Mechanics and CAS Center for Excellence in Ultra-intense Laser Science, Chinese Academy of Sciences, Shanghai 201800, China*

[2] *Center of Materials Science and Optoelectronics Engineering, University of Chinese Academy of Sciences, Beijing 100049, China*

[3] *Laser Fusion Research Center and Science & Technology on Plasma Physics Laboratory, China Academy of Engineering Physics, Mianyang 621999, China*

Abstract As intense, ultrashort, kHz-repetition-rate laser systems become commercially available, pulse cumulative effects are critical for laser filament based applications. In this work, the pulse repetition rate effect on the femtosecond laser filamentation in air was investigated both numerically and experimentally. The pulse repetition rate effect has negligible influence at the leading edge of filament. Clear intensity enhancement from high repetition pulse is observed at the peak and tailing edge of laser filament. As the repetition rate of the laser pulses increasing from 100Hz to 1000Hz, the length of filament extends and the intensity inside the filament increases. A physical picture based on the pulse repetition

This peer-reviewed article has been accepted for publication but not yet copyedited or typeset, and so may be subject to change during the production process. The article is considered published and may be cited using its DOI.

10.1017/hpl.2023.31

rate dependent “low density hole” effect on filamentation is proposed to well explain the obtained results.

Key words: femtosecond laser filamentation; cumulative effects; clamping intensity

I. INTRODUCTION

A nonlinear propagation known as filamentation is produced when intense femtosecond laser pulses propagate in air. The dynamic equilibrium between the Kerr self-focusing and plasma-defocusing effects leads to filamentation [1–3]. Due to its potential applications in supercontinuum emission [4–6], extreme ultraviolet (EUV) emission [7,8], air lasing [9,10], THz radiation [11,12], remote sensing [13], guiding of corona discharge [14], machining [15] and weather control [16], filamentation of femtosecond laser pulses in optically transparent media has attracted a lot of attentions in recent years. One of the most profound effects during femtosecond filamentation is the intensity clamping phenomena. It was observed in 1995 by Braun *et al*. [17] that the pulse energy inside a filament is generally constant within long propagation distance. Kasparian *et al*. [18] firstly proposed the intensity clamping in 2000. Intensity clamping has a significant impact on the diameter and length of the filament [19]. Gas density effect on filamentation has been investigated [20,21]. The simulation by Geints *et al*. [20] shows that lowering the air pressure in the focusing zone can improve the highest attainable laser pulse intensity by an order of magnitude. The molecular number density of a gas varies with pressure, changing medium properties and affecting the filamentation process. However, Couairon *et al*. [21] numerically investigated filamentation at various air pressures by varying the parameters of the pulse in the propagation model. They found clamping intensity is insensitive to the pressure. Pulse cumulative effect by high-repetition rate laser can also influence the local gas density along filamentation region. After filamentation, the plasma will recombine rapidly accompanied by the generation of shock waves and heat. Finally a “low density hole” is formed in the filament zone [22,23]. The low-density region will evolve at the rate of air molecules' thermal diffusion, i.e., for up to milliseconds [24]. The low density hole can be accumulated by pulses. As high-energy, ultrashort, high-repetition-rate laser systems become commercially available, research on cumulative effects at repetition rates up to the kHz range can be experimentally done. Cumulative effects on filament related applications of THz generation [25], wake dynamics [26] and the fluorescence [27] have been recently reported. However, the cumulative effect of laser repetition rate on the intensity inside the filament, which is important to understand and control the filament related applications, is still unclear.

In this work, we look into the problem of pulse repetition rate effect on filamentation by both numerical analysis and experimental investigation. It was found that the maximum intensity increases and the filament length extends as the laser repetition rate ranging from 100 Hz to 1000Hz. A physical picture based on “low density hole” dependent laser intensity inside the filament is proposed to explain the clamping intensity variation inside the filament generated by different repetition rate laser pulses. The clamping intensity of filament under different repetition

https://doi.org/10.1017/hpl.2023.31 Published online by Cambridge University Press

rates were experimentally measured in air. The experimental results are in a good agreement with the numerical results.

Correspondence to: T.-J. Wang and Y.X. Liu, No. 390 Qinghe Road, Jiading District,Shanghai, 201800, China. Email: tiejunwang@siom.ac.cn (T.-J. Wang); yaoxiangliu@siom.ac.cn(Y.X. Liu)

II. Numerical simulations and Results

In order to study the influence of low density hole generated by high repetition rate laser on the filamentation process in steady state, a numerical simulation of ultrashort laser pulse filamentation was performed by solving the nonlinear Schrödinger equation (NLSE) coupled with the electron density evolution equation. The equations are written as [28,29]:

$$\frac{\partial E}{\partial z} = i\frac{1}{2k_0}\Delta_\perp E - i\frac{k''}{2}\frac{\partial^2 E}{\partial t^2} + i\frac{\omega_0}{c}n_2 IE - \frac{\beta^K}{2}I^{K-1}E - \frac{\sigma}{2}(1+i\omega_0\tau)\rho E + ik_0\Delta nE \quad (1)$$

$$\frac{\partial \rho}{\partial t} = \frac{\beta^K}{K\hbar\omega_0}\left(1-\frac{\rho}{\rho_{air}}\right)I^K \quad (2)$$

Where E is the envelope of the electric field and is assumed to be cylindrical symmetrical around the propagation axis z. $k_0 = 2\pi/\lambda_0$, $\omega_0 = 2\pi c/\lambda_0$ are the center wave number and center angular frequency for the input laser pulse at the center wavelength $\lambda_0 = 800nm$, respectively. $I = c\varepsilon_0 n_0|E|^2/2$ is the intensity of the light field and ε_0 is the permittivity in free space. The right terms of Eq.(1) account for diffraction in the transverse plane, group velocity dispersion, Kerr effect, multiphoton absorption, plasma absorption and defocusing with electron density ρ [30], and the refractive index change induced by the preformed density hole.

The heating process caused by filamentation can be regarded as an isochoric (constant volume) process since the pulse transit time (~ps) and the thermalization time (~ps) are much shorter than the time scale of the air flow motion [31], the peak temperature variation ΔT_{peak} caused by the heat release from the plasma in air is written as [32]:

$$\Delta T_{peak}(z) = \frac{U\rho_{plasma}(r=0,z)}{c_v\rho_{at}} \quad (3)$$

Where $U = 14.6\text{eV}$ is the ionization potential energy for the air molecules. $\rho_{plasma}(z)$ is the longitudinal distribution of plasma density in the single-pulse case. c_v is the gas isochoric heat capacity per molecule. The ambient air under 1 atm can be approximately regarded as an ideal diatomic molecular gas and $c_v = 5k_B/2$. $k_B = 1.38\times10^{-23}\text{J/K}$ is Boltzmann constant. ρ_{at} is the neutral molecule density in the air under 1 atm.

The air density of the density hole induced by the energy deposition in the air is written as [33]:

$$\rho_{air}(z) = \rho_{at} - \Delta\rho_{air}^{peak}(z)\exp\left(-\frac{r^2}{R(z)^2}\right) \quad (4)$$

https://doi.org/10.1017/hpl.2023.31 Published online by Cambridge University Press

$$\Delta\rho_{air}^{peak}(\mathrm{z}) = \rho_{at}\frac{\Delta T_{peak}(z)R_0^2(z)}{(\Delta T_{peak}(\mathrm{z}) + T_a)R^2(z)} \tag{5}$$

Where $T_a = 300\mathrm{K}$ is the ambient air temperature, and $\mathrm{R(z)} = (R_0^2(\mathrm{z}) + 4\alpha\Delta t)^{1/2}$ is the radius of the density hole. The initial radius of the density hole $R_0(z)$ is the radial distribution of plasma density in HWHM at z position. Then the "low density hole" will evolve with the thermal diffusivity $\alpha = 0.19\mathrm{cm}^2/\mathrm{s}$ [33,34]. Δt is the pulse temporal spacing of the subsequent pulse.

The values given above correspond to the neutral molecule density of the air under 1 atm. Some of the parameters in Eq. (1) vary with the air density. The variations with the molecule density of air are as follows [21]:

$$\begin{gathered} n_2 = n_{2,0} \times \rho_{index},\ \tau = \tau_0/\rho_{index},\ \sigma = \sigma_0 \times \frac{\rho_{index}(1+\omega_0^2\tau_0^2)}{\rho_{index}^2+\omega_0^2\tau_0^2}, \\ \beta^{\mathrm{K}} = \beta_0^K \times \rho_{index},\ k'' = k_0'' \times \rho_{index} \end{gathered} \tag{6}$$

Where $\rho_{index} = \rho_{air}/\rho_{at}$ denotes the relative air density. In the case of the ambient air under 1 atm, $n_{2,0} = 3.2 \times 10^{-23}\mathrm{m}^2/\mathrm{W}$ is the nonlinear coefficient of the Kerr effect, $\tau_0 = 350\mathrm{fs}$ is the momentum transfer collision time, $\sigma_0 = 2 \times 10^{-24}\mathrm{m}^2$ is the cross-section for inverse bremsstrahlung, $\beta_0^K = 1.27 \times 10^{-160}\mathrm{m}^{17}/\mathrm{W}^9$ is the coefficient related to the multiphoton ionization, $k_0'' = 2 \times 10^{-29}\mathrm{s}^2/\mathrm{m}$ is the coefficient of group velocity dispersion.

The density hole induces the refractive index change, which is written as [34]:

$$\Delta n(z) = -\Delta n_m(z)\ \exp\left(-\frac{r^2}{R^2(z)}\right) \tag{7}$$

$$\Delta n_m(z) = (n_0 - 1)\ \frac{\Delta T_{peak}(\mathrm{z})}{T_a}\frac{R_0^2(z)}{R^2(z)} \tag{8}$$

Where $n_0 = 1.000275$ is the refractive index of the ambient air, and Δn_m is the maximal refractive index change [34].

To reduce computer processing time, the simulations begin at d = 5.2 cm before the linear (geometrical) focus [35]. The initial laser beam is assumed to be Gaussian, which can be expressed as:

$$E = E_0\exp(-r^2/w_0^2)\exp(-t^2/\tau_p^2)\exp(-ik_0r^2/2f) \tag{9}$$

Where $w_0 = w_f/(1 + d^2/z_f^2)^{1/2}$ and $\tau_p = 35\mathrm{fs}$ are the transverse waist and the duration of the Gaussian beam, respectively. $w_f = 7\mathrm{mm}$ is the beam waist (1/e) before the focus lens. $z_f = \pi w_f^2 n_0/\lambda_0$ is the Rayleigh length of the beam. $f = d + z_f^2/d$ is the curvature of the laser wave at the distance d before the linear focus.

The nonlinear Schrödinger equation (Eq. 1) was solved by a split-step Crank-Nicolson method [35]. Figure 1 shows the simulation results of the maximal intensity of the femtosecond laser pulse as a function of the propagation distance under laser repetition rates of 100 Hz and 1000 Hz. When the pulse energy is low, for example 0.1mJ, laser filament is not formed yet. The repetition rate effect appears mainly around geometrical focus (Figure 1(a)). When the pulse energy is high enough for filamentation, the effect appears not only around the peak but also on

https://doi.org/10.1017/hpl.2023.31 Published online by Cambridge University Press

the tailing edge of the filament (Figure 1(b)-1(d)). Compared with the result of the 100Hz laser pulse, the maximal intensity is higher for the 1000 Hz laser pulse at both the peak and tailing edge of the filament. While there is less influence at the leading edge of the filament. The length of the filament generated by the 1000 Hz laser pulse is longer than the one by the 100 Hz laser pulse (Figure 1).

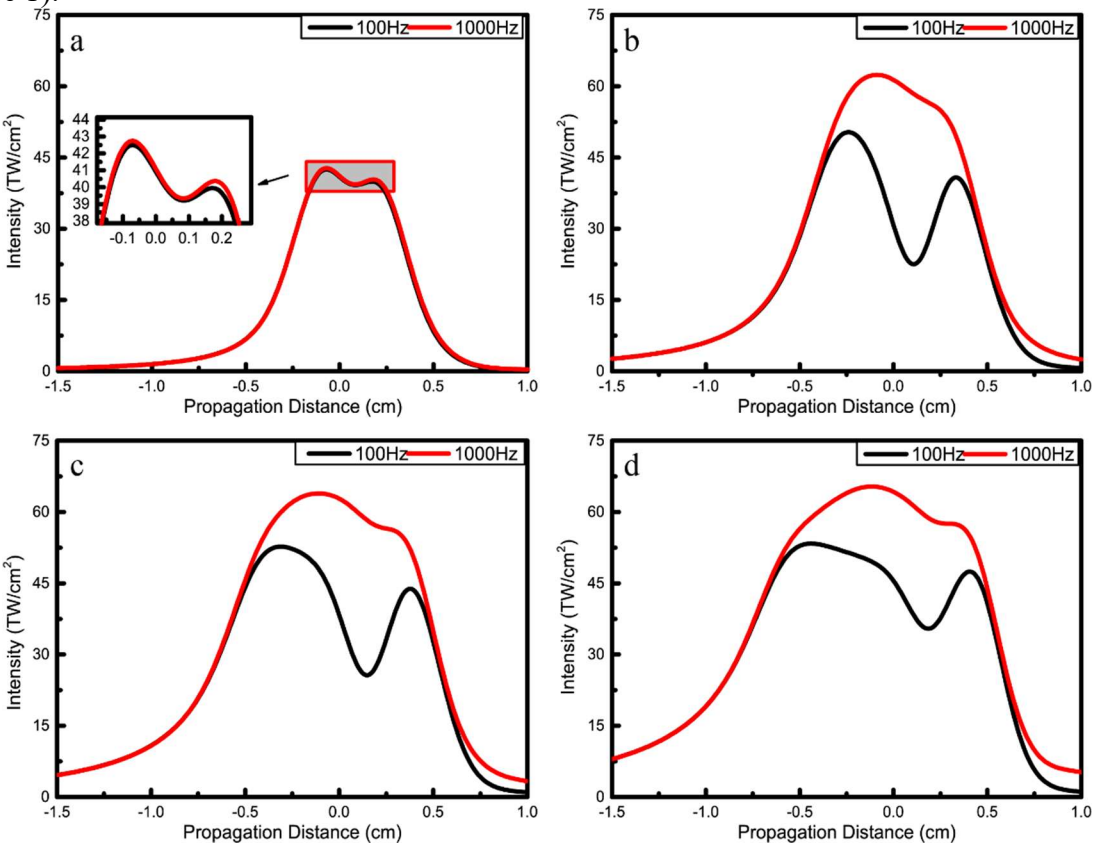

Figure 1. Maximal on-axis intensities of femtosecond laser pulses as a function of propagation distance for 100 Hz and 1000Hz repetition rates with different pulse energies of (a) 0.1mJ, (b) 0.2mJ, (c) 0.7mJ, (d) 1.2mJ. The geometric focus position is defined as 0 of the propagation distance and negative value is before the focus. The inset of (a) shows the enlargement of the shadow region of (a)

III. Experimental setup and results

https://doi.org/10.1017/hpl.2023.31 Published online by Cambridge University Press

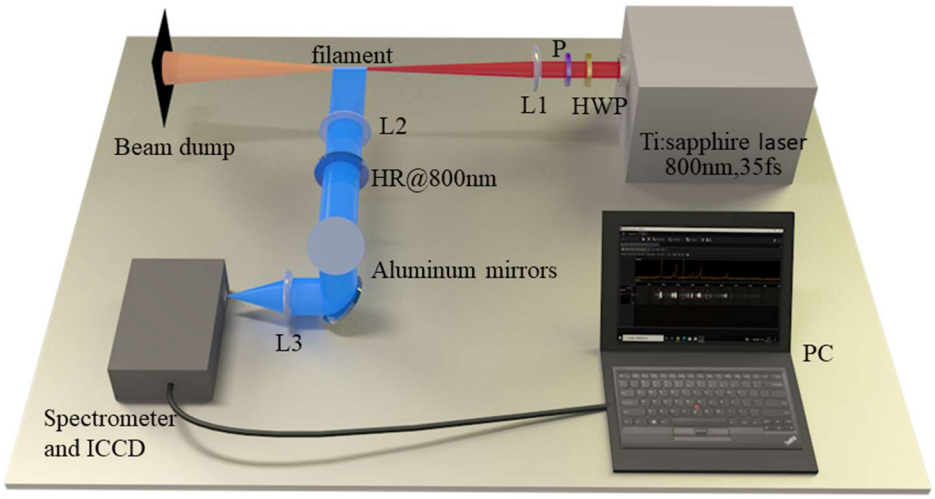

Figure 2. Experimental setup

In order to confirm the simulation results, the experiments of femtosecond laser filamentation in air under 100 Hz and 1000 Hz pulse repetition rates were performed. The simple fluorescence based method reported by Xu *et al*. [36] was adapted to estimate laser peak intensity inside the filament in air. The experimental setup is shown in Figure 2. A femtosecond laser pulse (800nm/4Hz~1kHz/35fs) generated by a Ti: sapphire (CPA) system (Spitfire Ace, Spectral-Physics) was focused by a fused silica convex lens L1 (f = 30 cm). The radius of the laser beam waist is about 7mm (1/e). The input energy of the laser pulse is continuously adjusted by a combination of a polarizer P and a half-wave plate HWP. The fluorescence emitted by the filament was imaged from the side by an imaging system of a pair of lenses L2 and L3 (30 cm and 10 cm focal lengths) and a pair of orthogonal ultraviolet-enhanced aluminum mirrors into the slit of a spectrometer. An ICCD mounted on the spectrometer trigged by the laser system was used to record the fluorescence spectrum generated from the filament. An energy meter (OPHIR PE50-DIF-C) inserted after L1 was employed to precisely monitor laser energy under different repetition rates.

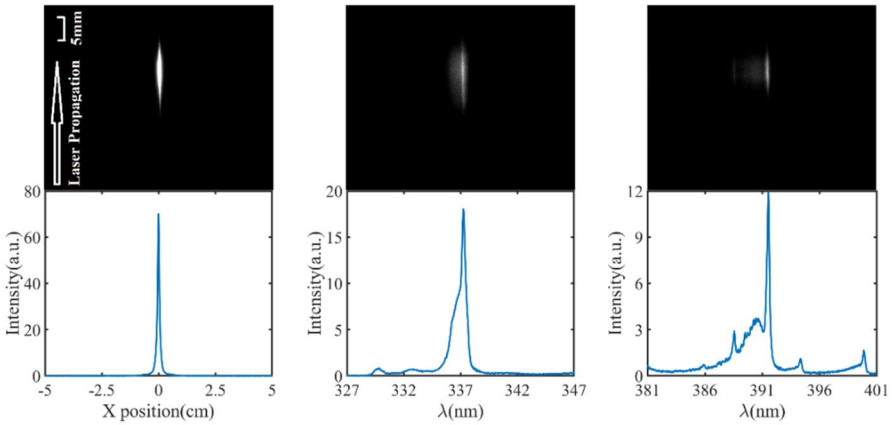

Figure 3. The typical spectrum images and intensity plots captured by the ICCD mounted on the spectrometer. (a) is in non-divided imaging mode. (b) and (c) are centered at the wavelengths of 337nm and 391nm. Laser pulse energy and repetition rate are 1.2 mJ and 1000 Hz, respectively.

https://doi.org/10.1017/hpl.2023.31 Published online by Cambridge University Press

The typical fluorescence images of laser filament on the ICCD are shown in Figure 3 for the laser pulse energy of 1.2 mJ and repetition rate of 1000 Hz, respectively. The images of the fluorescence spectra around 337 nm and 391 nm from the filament were acquired which were used for laser intensity estimation.

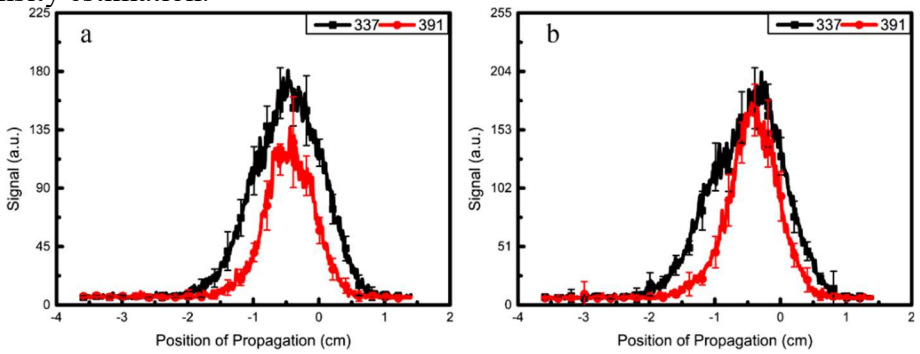

Figure 4. Longitudinal distribution of the nitrogen 337nm and 391nm fluorescence signal along filaments under filament repetition rates of (a) 100 Hz and (b) 1000Hz. The geometric focus position is defined as 0 of the propagation position and the negative values are before the focus. Laser pulse energy is 1.2mJ for filamentation.

The longitudinal distributions of two fluorescence lines in Figure 3 are shown in Figure 4 for laser repetition rates of 100 Hz and 1000 Hz, respectively. Laser pulse energy was fixed at1.2mJ. In Figure 4, the distance range that the 391nm fluorescence covers is smaller than that of the 337nm signal. The distance ranges of the two fluorescence signals are enlarged with the increasing repetition rate of laser pulses. The relevant effects of "density hole" induced by the previous pulse, such as thermal lens, will weaken the external focus and reduce the consumption of laser energy through air ionization. As a consequence, longer filaments as predicted in the simulation (Figure 1) were experimentally observed (Figure 4). Higher laser repetition rate, which means shorter pulse interval, leads to stronger effect on filament length.

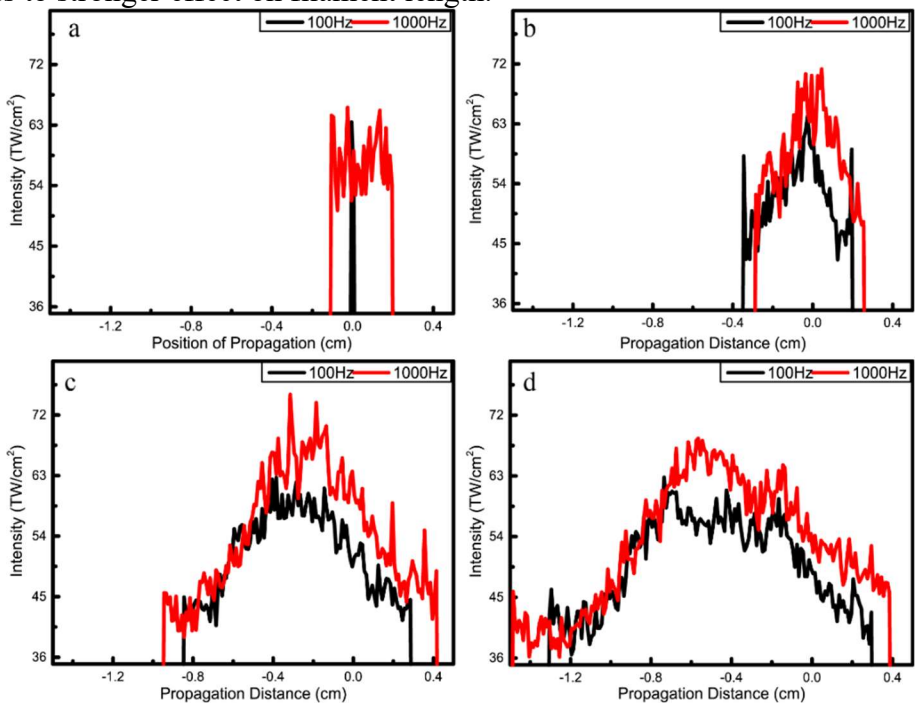

https://doi.org/10.1017/hpl.2023.31 Published online by Cambridge University Press

Figure 5. The laser peak intensities with different incident laser pulse energies (a) 0.1mJ, (b) 0.2mJ, (c) 0.7mJ, (d) 1.2mJ, under different laser repetition rates (black line:100Hz, red line:1kHz) as determined by Eq (10).

To characterize the laser intensity inside filament, we use the empirical formula reported in ref. [36], which is based on the 391nm and 337nm nitrogen fluorescence as followed:

$$I = 79 \times \left(\frac{2.6}{R} - 1\right)^{-0.34} \ \mathrm{TW/cm^2} \tag{10}$$

Where $\mathrm{R} \equiv \frac{S_{391}}{S_{337}} \propto \frac{aI^{n_1}}{aI^{n_1}+bI^{n_2}}$ is intensity ratio between the two fluorescence lines. I is the pulse peak intensity, and n_1, n_2 are the effective orders of nonlinearity of ionizing the molecule into the excited or ground state ions. a, b are the proportionality constants. The laser peak intensity could be calculated using the value of R through Eq. (10). Figure 5 depicts the experimentally measured laser peak intensity as a function of propagation under different laser pulse energies of 0.1mJ, 0.2mJ, 0.7mJ and 1.2mJ, respectively. At the low energy of 0.1mJ, the fluorescence-based intensity estimation method does not reproduced the simulation prediction due to the weak fluorescence excited at the small energy (Figure 5(a)). Once laser pulse energy is high enough for filamentation, the predicted intensity behaviors under 100Hz and 1000Hz pulse repetition rates are well reproduced (Figure 5(b)-6(d)). No clear differences on intensity at the leading edges of filaments were observed which agrees with the simulation results in Figure 1(b)-1(d). During the filamentation process, the laser peak intensity is approximately $70\ \mathrm{TW/cm^2}$. The laser peak intensity is stronger and the filamentation zone is enlarged when using a higher laser repetition rate of 1000 Hz. The experimental results are well consistent with the numerical simulations based on the NLSE.

https://doi.org/10.1017/hpl.2023.31 Published online by Cambridge University Press

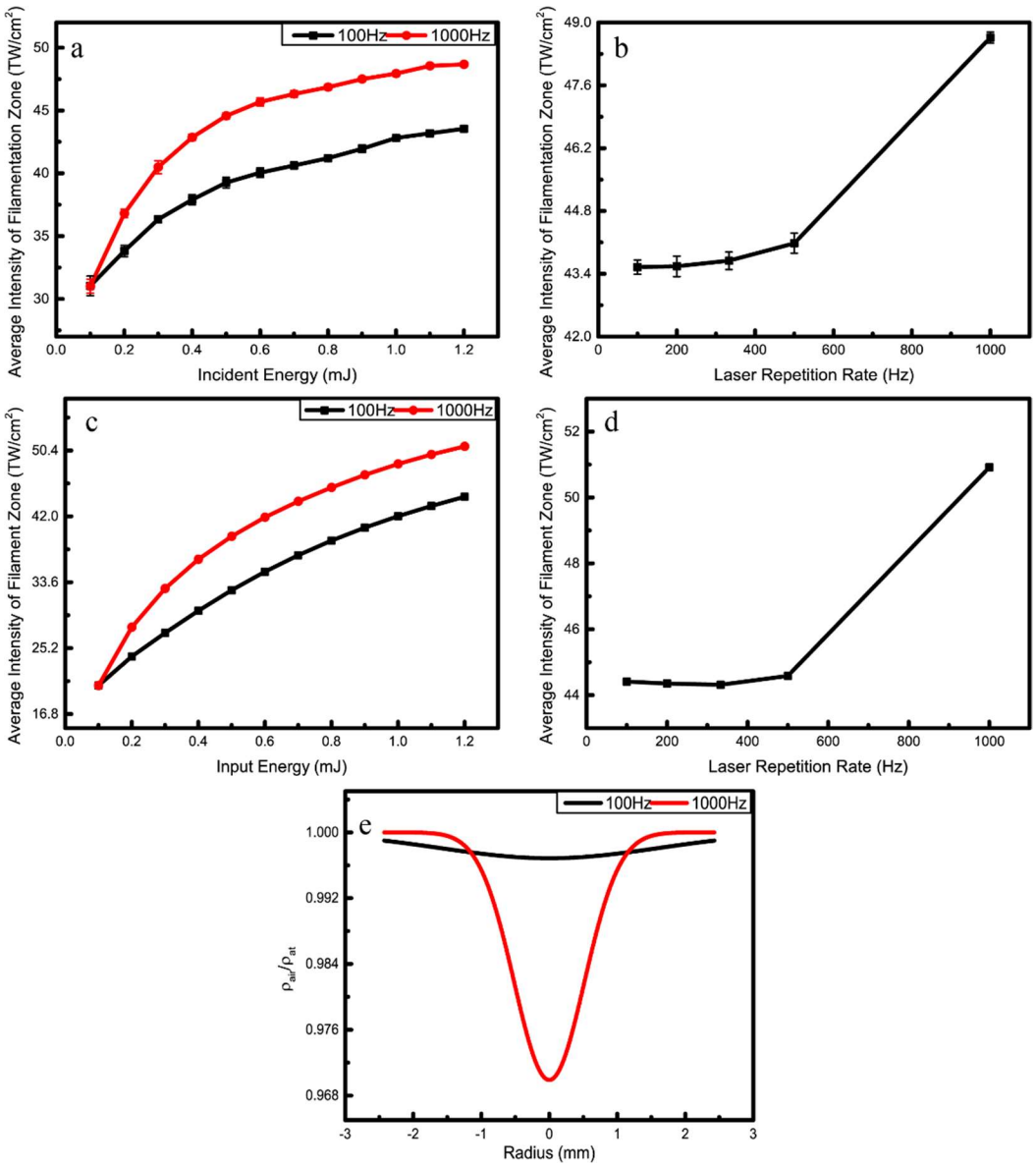

Figure 6. Experimentally measured average intensity of the filament as a function of (a) incident energy, (b) laser repetition rate (The incident energy is 1.2 mJ). The filament range is defined by specifying the filamentation initiation and termination when the total fluorescence intensity approaches 1/e of the maximum intensity. (c) Numerically obtained average intensity of filamentation zone as a function of incident energy for laser repetition rates of 100 Hz and 1000 Hz. (d) Numerically obtained average intensity of filamentation zone as a function of laser repetition rates for incident energy of 1.2mJ. (e) The radial distributions of the gas density hole generated by 100 Hz and 1000 Hz repetition rate lasers.

Figure 6(a) depicts the experimentally acquired average intensity of the filamentation zone for all incident energies. The filament zone is defined by specifying the filamentation initiation and termination when the total fluorescence intensity approaches 1/e of the maximum intensity. The intensity tends to be saturated because of clamping effect when the incident energy increases. Furthermore, the obtained intensities of 1 kHz filament are higher than that of 100Hz. Figure 6(b) summarizes the average intensity of the filamentation zone, demonstrating the intensity inside the filament as a function of the laser repetition rate. As for a comparison the numerically obtained average intensity of the filamentation zone as a function of laser input energy is shown in Figure

https://doi.org/10.1017/hpl.2023.31 Published online by Cambridge University Press

6(c). Both experimental and theoretical results show that the average intensity of the 1000 Hz filament is clearly higher than that of 100 Hz filament. The difference enlarges as the laser pulse energy increases. The experimental results are in good agreement with that predicted by the simulation in Figure 6(c)(d) which confirms that the repetition rate dependent low density hole plays the significant role during filamentation in air.

The effect of pulse repetition rate on filamentation can be understood as the following. After the recombination of the plasmas inside the filament zone, part of laser pulse energy is deposited into air molecules resulting in thermal diffusion along the radial direction. As a consequence, a low-density hole in air is established. The density hole decays in milliseconds timescale [24] and the next pulse will "see" it if the pulse interval time shorter than the density hole lifetime. The "density hole" impacts the laser filament in two ways. One is to change the spatial distribution of the air refractive index. The refractive index distribution structure acts like a defocus lens, namely thermal lens, weakening the focus of the succeeding laser pulse. The other is to influence other parameters of air medium, such as the nonlinear Kerr effect coefficient, the momentum transfer collision time, the cross-section for inverse bremsstrahlung, the coefficient linked to multiphoton ionization, and the coefficient of group velocity dispersion. These parameters play an important role in laser pulse nonlinear propagation (Eq. 1). The time for the "density hole" to decay is of 1ms and 10ms for laser repetition rates at 1 kHz and 100 Hz, respectively. The radius of the steady "density hole" is smaller for 1 kHz (Figure 6. (e)), which induces larger maximum refractive shifts. The density hole caused by the previous pulse at 1000Hz is sharper than that at 100Hz, due to the shorter pulse interval time of 1ms as shown in Figure 6(e). The next subsequent pulse propagating in the region experiences a smaller nonlinear refractive index coefficient and lower ionization rate for higher repetition rate laser. As a consequence, less energy is consumed by tunneling/multiphoton ionization and thus more energy is confined in the filament region. Therefore, the clamped intensity of the laser filaments increases when using higher repetition rate laser (Figure 6 (a)-(d)). At the leading edge of filament, plasma density is not that high as compared with that at the peak and the tailing of the filament. Therefore less energy is deposited in the region through plasma recombination leading to very weak thermal lensing effect. This could contribute the less laser repetition influence at the leading edge of filaments in Figure 1. The peak power at the position of previous filament tail is still high enough for self-focusing as well as for filamentation, which leads to the extension of filament length at the tail end both experimentally and theoretically.

It is noted that more recently Isaacs *et al*. [37] developed a model describing pulse train isobaric heating air, and simulated the propagation of a high-power pulse train at 1 kHz repetition rate. The similar results of the filament length are predicted by the model when pulse cumulative effect is considered. However, no obvious change of the peak intensity inside the laser filament was predicted since the only refractive index change caused by the "low density hole" was considered in the model.

IV. Conclusion

In summary, the theoretical and experimental investigation on pulse repetition rate dependent laser filamentation in air were performed. The numerical prediction results by solving the nonlinear Schrödinger equation reveal that the maximum intensity inside the filament is higher and the length of the filament is longer for 1000Hz laser pulse compared with the result by the 100 Hz pulse. The

https://doi.org/10.1017/hpl.2023.31 Published online by Cambridge University Press

pulse repetition rate effect has negligible influence at the leading edge of laser filament. Clear intensity enhancement from high repetition pulse is observed at the peak and tailing edges of laser filament. The formation of "low density hole" after filamentation by the last pulse leads to defocusing effect and lower ionization rate. For laser pulses at high repetition rate, the density hole caused by the previous pulse is sharper than that at low repetition rate due to the shorter pulse interval time. Consequently, the clamped laser intensity of the laser filaments is higher with a higher repetition rate. Direct experimental measurements of the laser peak intensity of different incident laser pulse energies under different laser repetition rates were performed via the side fluorescence of the filament. Using the image of the spectrum of the side fluorescence from the filament, the longitudinal distribution of the laser peak intensity of the filament was resolved. The experimental results are in a good agreement with numerical predictions. We believe that the results presented in this work are useful not only for further understanding the laser repetition effect on the laser filamentation in air but also for the related applications.

Acknowledgement

The work was in part supported by NSAF (Grant No. U2130123), International Partnership Program of Chinese Academy of Sciences (Grant No. 181231KYSB20200033 and 181231KYSB20200040), Shanghai Science and Technology Program (Grant No.21511105000).

References

1. S. L. Chin, S. A. Hosseini, W. Liu, Q. Luo, F. Théberge, N. Aközbek, A. Becker, V. P. Kandidov, O. G. Kosareva, and H. Schroeder, "The propagation of powerful femtosecond laser pulses in opticalmedia: physics, applications, and new challenges," Canadian Journal of Physics **83**, 863–905 (2005).
2. S. L. Chin, T.-J. Wang, C. Marceau, J. Wu, J. S. Liu, O. Kosareva, N. Panov, Y. P. Chen, J.-F. Daigle, S. Yuan, A. Azarm, W. W. Liu, T. Seideman, H. P. Zeng, M. Richardson, R. Li, and Z. Z. Xu, "Advances in intense femtosecond laser filamentation in air," Laser Phys. **22**, 1–53 (2012).
3. A. Couairon and A. Mysyrowicz, "Femtosecond filamentation in transparent media," Physics Reports **441**, 47–189 (2007).
4. L. Bergé, S. Skupin, G. Méjean, J. Kasparian, J. Yu, S. Frey, E. Salmon, and J. P. Wolf, "Supercontinuum emission and enhanced self-guiding of infrared femtosecond filaments sustained by third-harmonic generation in air," Phys. Rev. E **71**, 016602 (2005).
5. A. K. Dharmadhikari, S. Edward, J. A. Dharmadhikari, and D. Mathur, "On the generation of polarization-dependent supercontinuum and third harmonic in air," J. Phys. B: At. Mol. Opt. Phys. **48**, 094012 (2015).
6. N. Chen, T.-J. Wang, Z. Zhu, H. Guo, Y. Liu, F. Yin, H. Sun, Y. Leng, and R. Li, "Laser ellipticity-dependent supercontinuum generation by femtosecond laser filamentation in air," Opt. Lett. **45**, 4444 (2020).

https://doi.org/10.1017/hpl.2023.31 Published online by Cambridge University Press

7. N. Aközbek, A. Iwasaki, A. Becker, M. Scalora, S. L. Chin, and C. M. Bowden, "Third-Harmonic Generation and Self-Channeling in Air Using High-Power Femtosecond Laser Pulses," Phys. Rev. Lett. **89**, 143901 (2002).
8. D. Wang, W. Li, L. Ding, and H. Zeng, "Enhanced XUV pulse generation at 89 nm via nonlinear interaction of UV femtosecond filaments," Opt. Lett. **39**, 4140 (2014).
9. L. Yuan, Y. Liu, J. Yao, and Y. Cheng, "Recent Advances in Air Lasing: A Perspective from Quantum Coherence," Adv Quantum Tech **2**, 1900080 (2019).
10. P. Polynkin and Y. Cheng, eds., *Air Lasing*, Springer Series in Optical Sciences (Springer International Publishing, 2018), Vol. 208.
11. T.-J. Wang, J. Ju, Y. Liu, R. Li, Z. Xu, and S. Leang Chin, "Waveform control of enhanced THz radiation from femtosecond laser filament in air," Appl. Phys. Lett. **110**, 221102 (2017).
12. C. D'Amico, A. Houard, M. Franco, B. Prade, A. Mysyrowicz, A. Couairon, and V. T. Tikhonchuk, "Conical Forward THz Emission from Femtosecond-Laser-Beam Filamentation in Air," Phys. Rev. Lett. **98**, 235002 (2007).
13. H. L. Xu, J. F. Daigle, Q. Luo, and S. L. Chin, "Femtosecond laser-induced nonlinear spectroscopy for remote sensing of methane," Appl. Phys. B **82**, 655–658 (2006).
14. Y. Wei, Y. Liu, T.-J. Wang, N. Chen, J. Ju, Y. Liu, H. Sun, C. Wang, J. Liu, H. Lu, S. L. Chin, and R. Li, "Spectroscopic analysis of high electric field enhanced ionization in laser filaments in air for corona guiding," High Pow Laser Sci Eng **4**, e8 (2016).
15. C. Hnatovsky, V. Shvedov, W. Krolikowski, and A. Rode, "Revealing Local Field Structure of Focused Ultrashort Pulses," Phys. Rev. Lett. **106**, 123901 (2011).
16. J. Ju, T. Leisner, H. Sun, A. Sridharan, T.-J. Wang, J. Wang, C. Wang, J. Liu, R. Li, Z. Xu, and S. L. Chin, "Laser-induced supersaturation and snow formation in a sub-saturated cloud chamber," Appl. Phys. B **117**, 1001–1007 (2014).
17. A. Braun, G. Korn, X. Liu, D. Du, J. Squier, and G. Mourou, "Self-channeling of high-peak-power femtosecond laser pulses in air," OPTICS LETTERS **20**, 3 (1995).
18. J. Kasparian, R. Sauerbrey, and S. L. Chin, "The critical laser intensity of self-guided light filaments in air:," Appl Phys B **71**, 877–879 (2000).
19. S. Hosseini, O. Kosareva, N. Panov, V. P. Kandidov, A. Azarm, J.-F. Daigle, A. B. Savel'ev, T.-J. Wang, and S. L. Chin, "Femtosecond laser filament in different air pressures simulating vertical propagation up to 10 km," Laser Phys. Lett. **9**, 868–874 (2012).
20. Y. E. Geints, A. A. Zemlyanov, A. A. Ionin, S. I. Kudryashov, L. V. Seleznev, D. V. Sinitsyn, and E. S. Sunchugasheva, "Nonlinear propagation of a high-power focused femtosecond laser pulse in air under atmospheric and reduced pressure," Quantum Electron. **42**, 319–326 (2012).
21. A. Couairon, M. Franco, G. Méchain, T. Olivier, B. Prade, and A. Mysyrowicz, "Femtosecond filamentation in air at low pressures: Part I: Theory and numerical simulations," Optics Communications **259**, 265–273 (2006).
22. J. K. Wahlstrand, N. Jhajj, E. W. Rosenthal, S. Zahedpour, and H. M. Milchberg, "Direct imaging of the acoustic waves generated by femtosecond filaments in air," Opt. Lett. **39**, 1290 (2014).
23. N. Jhajj, Y.-H. Cheng, J. K. Wahlstrand, and H. M. Milchberg, "Optical beam dynamics in a gas repetitively heated by femtosecond filaments," Opt. Express **21**, 28980 (2013).

https://doi.org/10.1017/hpl.2023.31 Published online by Cambridge University Press

24. G. Point, C. Milián, A. Couairon, A. Mysyrowicz, and A. Houard, "Generation of long-lived underdense channels using femtosecond filamentation in air," J. Phys. B: At. Mol. Opt. Phys. **48**, 094009 (2015).
25. A. D. Koulouklidis, C. Lanara, C. Daskalaki, V. Yu. Fedorov, and S. Tzortzakis, "Impact of gas dynamics on laser filamentation THz sources at high repetition rates," Opt. Lett. **45**, 6835 (2020).
26. A. Higginson, Y. Wang, H. Chi, A. Goffin, I. Larkin, H. M. Milchberg, and J. J. Rocca, "Wake dynamics of air filaments generated by high-energy picosecond laser pulses at 1 kHz repetition rate," Opt. Lett. **46**, 5449 (2021).
27. J. Xue, N. Zhang, L. Guo, Z. Zhang, P. Qi, L. Sun, C. Gong, L. Lin, and W. Liu, "Effect of laser repetition rate on the fluorescence characteristic of a long-distance femtosecond laser filament," Opt. Lett. **47**, 5676 (2022).
28. J. Chang, D. Li, L. Xu, L. Zhang, T. Xi, and Z. Hao, "Elongation of filamentation and enhancement of supercontinuum generation by a preformed air density hole," Opt. Express **30**, 16987 (2022).
29. A. Couairon, E. Brambilla, T. Corti, D. Majus, O. de J. Ramírez-Góngora, and M. Kolesik, "Practitioner's guide to laser pulse propagation models and simulation: Numerical implementation and practical usage of modern pulse propagation models," Eur. Phys. J. Spec. Top. **199**, 5–76 (2011).
30. E. Yablonovitch and N. Bloembergen, "Avalanche Ionization and the Limiting Diameter of Filaments Induced by Light Pulses in Transparent Media," Phys. Rev. Lett. **29**, 907–910 (1972).
31. G. Point, E. Thouin, A. Mysyrowicz, and A. Houard, "Energy deposition from focused terawatt laser pulses in air undergoing multifilamentation," Opt. Express **24**, 6271 (2016).
32. Q. Zeng, L. Liu, J. Ju, S. Hu, and K. Zhang, "Numerical investigation on the heat deposition characteristics of femtosecond laser pulses undergoing multiple filaments," Phys. Scr. **95**, 085605 (2020).
33. Y.-H. Cheng, J. K. Wahlstrand, N. Jhajj, and H. M. Milchberg, "The effect of long timescale gas dynamics on femtosecond filamentation," Opt. Express **21**, 4740–4751 (2013).
34. J. K. Wahlstrand, N. Jhajj, and H. M. Milchberg, "Controlling femtosecond filament propagation using externally driven gas motion," Opt. Lett. **44**, 199 (2019).
35. H. Guo, T.-J. Wang, X. Zhang, C. Liu, N. Chen, Y. Liu, H. Sun, B. Shen, Y. Jin, Y. Leng, and R. Li, "Direct measurement of radial fluence distribution inside a femtosecond laser filament core," Opt. Express **28**, 15529 (2020).
36. S. Xu, X. Sun, B. Zeng, W. Chu, J. Zhao, W. Liu, Y. Cheng, Z. Xu, and S. L. Chin, "Simple method of measuring laser peak intensity inside femtosecond laser filament in air," Opt. Express **20**, 299 (2012).
37. J. Isaacs, B. Hafizi, L. A. Johnson, E. W. Rosenthal, L. Mrini, and J. Peñano, "Modeling the propagation of a high-average-power train of ultrashort laser pulses," Opt. Express **30**, 22306 (2022).

https://doi.org/10.1017/hpl.2023.31 Published online by Cambridge University Press